Matter and Radiation at Extremes

RESEARCH ARTICLE | JULY 08 2024

Bunching enhancement for coherent harmonic generation by using phase merging effects

Ke Feng ; Kangnan Jiang ; Runshu Hu; Shixia Luan ; Wentao Wang ; Ruxin Li

Matter Radiat. Extremes 9, 057201 (2024)
https://doi.org/10.1063/5.0191508

Matter and Radiation at Extremes

RESEARCH ARTICLE

pubs.aip.org/aip/mre

Bunching enhancement for coherent harmonic generation by using phase merging effects

Cite as: Matter Radiat. Extremes 9, 057201 (2024); doi: 10.1063/5.0191508
Submitted: 14 December 2023 • Accepted: 31 May 2024 •
Published Online: 8 July 2024

Ke Feng,[1,a)] Kangnan Jiang,[1,2] Runshu Hu,[1,3] Shixia Luan,[1] Wentao Wang,[1,a)] and Ruxin Li[1,2]

AFFILIATIONS

[1] State Key Laboratory of High Field Laser Physics and CAS Center for Excellence in Ultra-intense Laser Science, Shanghai Institute of Optics and Fine Mechanics (SIOM), Chinese Academy of Sciences (CAS), Shanghai, People's Republic of China
[2] School of Physical Science and Technology, ShanghaiTech University, Shanghai, People's Republic of China
[3] Center of Materials Science and Optoelectronics Engineering, University of Chinese Academy of Sciences, Beijing, People's Republic of China

[a)] **Authors to whom correspondence should be addressed:** fengke@siom.ac.cn and wwt1980@siom.ac.cn

ABSTRACT

In this paper, promising but simple schemes are investigated to enhance the micro-bunching of relativistic electron beams for coherent harmonic generation (CHG) by using phase merging effects. In contrast to the standard CHG scheme, two specially designed dispersion sections (DSs) are adopted with the DS-modulator–DS configuration. The phase space of the *e* beam is appropriately coupled in the first DS, and the electrons within one seed wavelength can merge to the same phase with a matched second DS. Micro-bunching of the *e* beam can thus be enhanced by a large margin with much higher-harmonic components. Taking *e* beams from laser wakefield accelerators (LWFAs) as an example, start-to-end simulations are performed to show the effectiveness and robustness of the proposed schemes with several configurations. The beam current can be optimized to several tens to hundreds of kiloamperes, and the radiation power reaches hundreds of megawatts in the extreme ultraviolet regime within a 3.5 m-long beamline. The proposed schemes offer new opportunities for future compact free-electron lasers driven by LWFAs and provides prospects for truly compact and widely applicable systems.

I. INTRODUCTION

Free-electron lasers (FELs) are capable of delivering intense and coherent radiation with tunable wavelengths and are now established as unique high-brilliance tools for basic scientific investigations with atomic resolution at femto-to-attosecond timescales.[1–6] At X-ray wavelengths, FELs are typically based on the mechanism of self-amplified spontaneous emission (SASE). However, the SASE action produces photons with a limited longitudinal coherence, because the radiation starts from the random shot noise in the electron beam (*e* beam).[7,8] Prebunching *e* beams before injecting them into the FEL interaction region would produce fully coherent X rays, expedite the FEL amplification process, and enable high power and high energy extraction efficiency by tapering-enhanced superradiance.[9–12] However, owing to the lack of seeds at X-ray wavelengths, various harmonic seeding schemes for prebunching *e* beams have been proposed for superradiant FELs.[10] The high-gain harmonic-generation (HGHG) configuration[13–15] is the most representative of these, whereas for FELs with no exponential gain, the seeding scheme is referred to as coherent harmonic generation (CHG).[16–18] The standard CHG configuration consists of two undulators separated by a dispersive magnetic chicane. A seed laser interacts with the electrons to imprint a sinusoidal energy modulation at the scale of the seed laser wavelength into the *e* beam in the first undulator (modulator). This energy modulation evolves into a tight density modulation (bunching) with high-harmonic current components of the seed laser frequency in the following dispersive chicane. However, the energy modulation needs to be strengthened to obtain significant bunching at higher harmonics, and this will degrade the beam quality and result in a lower FEL power in the downstream undulator (radiator). To improve the frequency multiplication efficiency with a small induced energy spread, more complicated schemes such as multistage HGHG with the "fresh bunch" technique,[19,20] echo-enabled harmonic generation (EEHG),[21–25] and

phase-merging enhanced harmonic generation (PEHG)[26–28] have been studied extensively.

Benefitting from the unprecedented accelerating gradient of up to several hundreds of gigavolts per meter, laser wakefield accelerators (LWFAs) have considerable potential as alternative drivers for compact FELs.[29–37] Tremendous progress has been made in LWFA over the past decade, owing to extensive research on high-quality injection, acceleration, and laser guiding schemes.[31,38] It has proved possible to obtain e beams with energy of up to ~8 GeV,[39] emittance of the order of 0.1 mm mrad,[40,41] energy spread of a few per mille,[42,43] and beam charges of several nanocoulombs[44,45] with increasing stability.[46] Following the improvements in beam quality, lasing of an FEL adopting a LWFA has been demonstrated with both SASE[47] and seeded[48] configurations. Owing to the natural production of multi-kiloampere electron bunches in LWFA,[49,50] the pre-bunched schemes can further increase the bunch current to several tens or hundreds of kiloamperes. Such schemes offer new opportunities for coherent and intense radiation even without exponential gain in a sufficient short undulator[51,52] and hence open up prospects for truly compact and widely applicable systems.

In this paper, we investigate bunching-enhanced schemes using phase merging effects to significantly improve the frequency multiplication efficiency. The simulation and theoretical analysis presented here demonstrates that the dispersion section–modulator–dispersion section (DS-M-DS) configuration is a promising scheme. Benefitting from the phase-space coupling induced by the first dispersion section (DS-I), the modulated electrons in the beam can merge to the same phase within one seed wavelength after passing a matched second dispersion section (DS-II), and the bunching of the e beam can thus be increased significantly. As shown in Fig. 1, DS-I is used to couple the appropriate phase spaces among the electrons in the beam. Such coupling can be of transverse–longitudinal phase spaces (i.e., transverse position–energy or transverse momentum–energy) or transverse–transverse phase spaces (i.e., transverse position-transverse momentum), which can be chosen appropriately with the designed e-beam parameter to obtain the maximum up-conversion efficiency. The following short modulator facilitates the generation of sinusoidal modulation (energy modulation[14,18] or angular modulation[53–55]) on the electrons while interacting with the seed laser. The modulated e beam is then sent to DS-II to realize conversion from energy modulation or angular modulation to density modulation. At the same time, electrons with different initial energy or divergence rapidly merge to the same phase within one seed wavelength, and the bunching factor increases significantly to realize a fully coherent FEL with shorter wavelength in the downstream radiator.

Start-to-end simulations with e beams from laser wakefield accelerators (LWFAs) are performed to demonstrate the feasibility of the proposed schemes. The results show that the harmonic number is increased significantly under optimized conditions, and the radiation power reaches the hundreds of megawatts level, with the total beamline within 3.5 m. The proposed schemes are universal and robust but easy to implement, and they have great potential for suitable applications with various e-beam sources, including LWFAs, storage rings (SRs),[56] and linear accelerators.[57]

II. PHYSICAL MECHANISM OF BUNCHING ENHANCEMENT

To give a theoretical analysis of the underlying physics of bunching enhancement, we adopt the vector $\vec{X} = (x, x', y, y', z, \delta)^T$ to character the state of the electrons in six-dimensional (6D) phase space, where x, y, and z are the horizontal, vertical, and longitudinal positions, x' and y' are the horizontal and vertical divergences, and $\delta = (\gamma - \gamma_0)/\gamma_0$ is the relative particle energy deviation with respect to the reference particle.[18] After passing through the linear Hamiltonian system, the state of the electron becomes $\vec{X}_1 = \mathbf{R}\vec{X}_0$, where $\mathbf{R}$ is a 6 × 6 transfer matrix describing the beam dynamics. DS-I is placed behind the accelerator and can be designed to introducing whichever of the relative coupling coefficients R_{12}, R_{16}, and R_{26} needs to be optimized according to the actual e-beam parameter. The corresponding coefficient can be expressed in a more general form as R_{ij} (i, j = 1, 2, 6 and $i < j$), which represents the coupling between X_i and X_j of the beam. It should be noted that the aforementioned analysis is also applicable to the vertical coordinates, but this is ignored for brevity here. After interacting with the seed laser, the e beam is sinusoidally modulated in the modulator. The modulation corresponds to angular modulation[53–55] for the case of i = 1 and j = 2. In other cases, it is energy modulation.[14,18] Following the modulator is DS-II, which can be specially designed for introducing R_{5i} and R_{5j} to convert the energy or angular modulation to density modulation and enhance the bunching simultaneously. In fact, the desired coupling can be designed as a whole with beam transport devices (e.g., dipole magnets) or their combinations,[58] and the specific beamlines using an e beam from an LWFA will be discussed in Sec. III.

To illustrate the underlying physics more clearly, we set i = 1 and j = 6 as a simple example here. The element of the transfer matrix

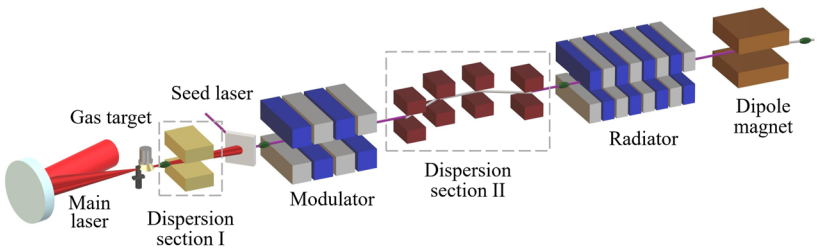

FIG. 1. Schematic layout of the bunching enhanced scheme for coherent harmonic generation with the DS-M-DS configurations. The dispersion Sec. I and dispersion Sec. II, indicated by the dashed boxes, need to be designed specifically for a given e beam.

induced by DS-I is R_{16}, corresponding to transverse dispersion of the beam. The normalized variables $p = (\gamma - \gamma_0)/\sigma_\gamma$ and $\chi = (x - x_0)/\sigma_x$ are adopted to describe the dimensionless energy deviation and horizontal position of the electrons with average energy $\gamma_0 mc^2$ and central beam position x_0,[18] where σ_γ and σ_x are the root mean square (rms) energy spread and horizontal beam size at the entrance of DS-I, respectively. The initial distributions for p and χ are assumed to be $f_0(p) = N_0(2\pi)^{-1/2}e^{-p^2/2}$ and $g_0(\chi) = N_0(2\pi)^{-1/2}e^{-\chi^2/2}$, where N_0 is the number of electrons per unit length in the beam. After passing through DS-I, the horizontal position of the beam is changed to $\chi_1 = \chi + (R_{16}\sigma_\delta/\sigma_x)p$, where $\sigma_\delta = \sigma_\gamma/\gamma_0$ represents the relative energy spread of the beam. The e beam is energy-modulated during the interaction with the seed laser in the modulator, with a modulation amplitude $A = \Delta\gamma/\sigma_\gamma = 2K_0L_uJ\sqrt{P_L/P_0}/(\gamma w_0\sigma_\gamma)$ induced by a plane electromagnetic wave. Here, $\Delta\gamma$ is the modulation depth, σ_γ is the rms energy spread of the e beam, P_L and w_0 are the peak power and the radius of the seed laser, $P_0 = I_A mc^2/e^2 = 8.7$ GW, $I_A \approx 17$ kA is the Alfvén current, K_0 and L_u are the parameter and the total length of the undulator, and $J = J_0\left(K_0^2/(4+2K_0^2)\right) - J_1\left(K_0^2/(4+2K_0^2)\right)$.[18] The dimensionless energy deviation evolves to $p_1 = p + A\sin(k_s z)$ at the exit of the modulator, where k_s is the wavelength of the seed laser. After its injection into the following DS-II, the corresponding longitudinal position of the beam evolves to

$$z_1 = z + R_{51}\sigma_x\left(\chi + \frac{R_{16}\sigma_\delta}{\sigma_x}p\right) + R_{56}\sigma_\delta[p + A\ \sin(k_s z)], \quad (1)$$

where z and z_1 are the longitudinal positions of the beam at the beginning and end of the beamline, respectively. For large coupling coefficient R_{16} and modulation amplitude A, the small factor χ and p can be omitted, and a clearer physical picture can be obtained from Eq. (1), which simplifies to

$$z_1 = z + R_{51}R_{16}\sigma_\delta p + R_{56}\sigma_\delta A\ \sin(k_s z). \quad (2)$$

The first term on the right-hand side of Eq. (2) is the initial longitudinal position of an electron in the beam, and the third term represents the conversion of the sinusoidal energy modulation to a density modulation with an appropriate R_{56}, as shown in Figs. 2(a) and 2(b). The important second term shows linear correlations with the initial normalized energy derivation p. It indicates that electrons with different initial energies will have different longitudinal displacements and can merge to the same longitudinal position within one seed wavelength range, as long as appropriate coupling coefficients R_{51} and R_{16} are chosen, as shown in Figs. 2(c) and 2(d). The up-conversion efficiency is expected to be enhanced significantly through exploitation of the bunching enhancement technique using phase merging effects.

The density modulation of the e beam can be quantified by the bunching factor, which is defined as $b = \langle e^{-i\theta_j}\rangle$, where $\theta_j = (k_s + k_u)z - ck_s t$ is the pondermotive phase for particle j in the beam, the angular brackets indicate the average after summing over particles in the beam, and k_u is the wavenumber of the undulator. According to the bunching factor for the PEHG scheme in Ref. 26, the bunching

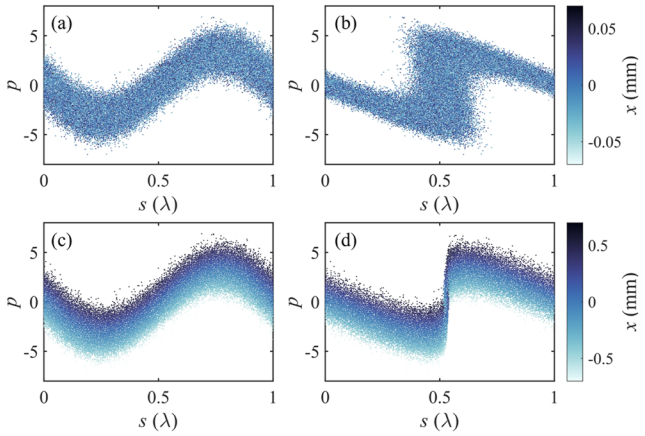

FIG. 2. Schematic of standard CHG and bunching enhanced CHG schemes: (a) and (c) x–z–p phase-space distributions of the e beam at the exit of the modulator in the standard CHG and bunching enhanced CHG schemes, respectively; (b) and (d) x–z–p phase-space distributions of the e beam at the entrance of the radiator in the standard CHG and bunching enhanced CHG schemes, respectively. The initial horizontal size and energy spread of the e beam are assumed to be 1 μm and 0.1%, respectively. The coupling coefficient R_{16} induced by DS-I is 2 cm, and the amplitude of energy modulation is $A = 3$. The corresponding coupling coefficients induced by DS-II are $R_{51} = 2.2 \times 10^{-4}$ and $R_{56} = -4.7 \times 10^{-5}$ m.

factor for the nth harmonic in the scheme presented here can be expanded to a more general form as follows:

$$b_n = J_n(nAk_sR_{5j}\sigma_j)\exp\left\{-\frac{1}{2}[nk_s(R_{5i}R_{ij} + R_{5j})\sigma_j]^2\right\} \times \exp\left[-\frac{1}{2}(nk_sR_{5i}\sigma_i)^2\right] \quad (i,j = 1,2,6; i < j), \quad (3)$$

where σ_i and σ_j are the corresponding rms values of the e-beam 6D phase spaces at the entrance of DS-I. To maximize the bunching shown in Eq. (3), the condition $R_{5i}R_{ij} + R_{5j} = 0$ needs to be satisfied, and the corresponding bunching factor is rewritten as

$$b_n = J_n(nAk_sR_{5j}\sigma_j)\exp\left[-\frac{1}{2}\left(nk_sR_{5j}\frac{\sigma_i}{R_{ij}}\right)^2\right] \quad (i,j = 1,2,6; i < j). \quad (4)$$

Typically, the Bessel function in Eq. (3) reaches its maximum value of $0.67/n^{1/3}$ when its argument equals $n + 0.81n^{1/3}$,[26] and the optimized coefficient is determined as $R_{5j} = (n + 0.81n^{1/3})/(nAk_s\sigma_j)$ for a given modulation amplitude A. Thus, the bunching factor is mainly determined by σ_i/R_{ij} in the exponential attenuation term. By choosing a relatively small σ_i along with a large coupling coefficient R_{ij} in DS-I, a considerable bunching factor can be obtained here. In particular, for the case of $R_{5i} = 0$ and $j = 6$, Eq. (3) can be rewritten as

$$b_n = J_n(nAk_sR_{56}\sigma_\delta)\exp\left[-\frac{1}{2}(nk_sR_{56}\sigma_\delta)^2\right], \quad (5)$$

which corresponds to the bunching factor for a standard CHG scheme.

As noted in the above analysis, the bunching factor for the standard CHG scheme is mainly determined by the energy spread of

the beam σ_δ and will lead to a low up-conversion efficiency for an e beam with a large energy spread. Using an intense seed laser to increase the modulation depth may be an alternative way to promote bunching in the standard CHG scheme, but the gain will be degraded accordingly, owing to the large energy modulation. On comparing the exponential attenuation terms in Eqs. (4) and (5), it can be seen that σ_δ in the latter is replaced by σ_i/R_{ij} in the former, which indicates that the presented scheme may be a superior method to obtain the optimum bunching for e beams even with different characteristics. It is believed that such a bunching enhanced technique provides another promising way for e beams from a variety of the sources to generate intense coherent radiation with short wavelength. In Sec. III, we take the e beams from LWFAs as examples to demonstrate the effective operation of the proposed scheme with various configurations.

III. START-TO-END SIMULATION

A. Laser wakefield acceleration

To demonstrate the feasibility of the proposed scheme, the e beam from an LWFA is taken as an example and start-to-end simulations are performed. Such e beams typically work with an extremely low efficiency because of the relatively large energy spread (typically of the order of 1%) in a standard CHG scheme, but they are well suited for the proposed scheme. The spectral quasi-3D particle-in-cell (PIC) simulation code FBPIC[59,60] is applied to gain insights into the acceleration stage. The simulation domain has sizes of 50 and 120 μm in the longitudinal and transverse directions, respectively, cell sizes of 31.25 and 80 nm in each direction and 16 macroparticles per cell. An 800 nm linearly polarized laser pulse with normalized vector potential $a_0 = 1.3$, waist radius $w_0 = 35$ μm, and pulse duration $\tau = 25$ fs is used to drive the wakefield. The density profile of the simulation is shown in Fig. 3(a), which is similar to that reported by Wang *et al.*[47] The evolution of the e-beam spectrum dQ/dE is also illustrated in Fig. 3(a). The slice properties of the e beam at the exit of the plasma are shown in Fig. 3(b). The simulated e beam has a peak energy of 525 MeV, a bunch charge of 30 pC, a global energy spread of 0.86% in rms (93% of the total electrons), and normalized projected emittances of 0.19 mm rad and 0.80 mm mrad in the horizontal and vertical directions, respectively.

B. Phase merging with normal dispersion

As illustrated in Sec. II, the coupling coefficient in DS-I can be chosen as R_{16} for a normal dispersion scheme, and the corresponding coefficients in DS-II are R_{51} and R_{56}. Generally, the horizontal dispersion can be introduced by exploiting a dog-leg composed of two dipoles or dog-leg schemes with quadrupoles inserted.[61] However, the bunch lengthening can be significant with LWFA-based e beams, which degrades the peak current and the FEL gain. A single-dipole scheme can be applied to provide the necessary dispersion, and the bunch lengthening can be minimized with an optimized beamline.[62] The coefficients R_{51} and R_{56} need to be introduced simultaneously in DS-II, which can be done by cascading a magnet dipole and a chicane, as illustrated in the Appendix [see Eq. (A2)]. For such a scheme, the coefficients are calculated as $R_{51} = b$ and $R_{56} = 2b_c^2 L_c$, where b and b_c are the bending angles for the dipole and chicane, respectively, and L_c is the drift length between each dipole in the chicane. It should be noted that the coefficients R_{51} and R_{56} can be optimized separately, which makes the presented scheme more feasible for use with different e-beam sources.

The total beamline and the associated evolution of the e-beam Twiss parameters along the beamline are shown in Fig. 4(a). After leaving the plasma, the e beam is focused by the quadrupole triplet, which consists two 5 cm-long quadrupoles and a 10 cm-long quadrupole with adjustable gradient. The subsequent DS-I stage consists of a dipole with a deflection angle of 0.05 rad and a length of 10 cm and a 10 cm-long quadrupole electromagnet to provide the appropriate coefficient R_{16} of 1.75 cm required for the following phase merging stage. The e beam is tracked through the beam line using the Ocelot code[63] with space charge and second-order transport effects taken into consideration. Similar results can be obtained using the Astra code.[64] The initial beam used for tracking is obtained from the output of the FBPIC code. After passing through DS-I, a four-period modulator with period length 5 cm is inserted, where the dispersed e beam interacts with a 266 nm seed laser pulse with

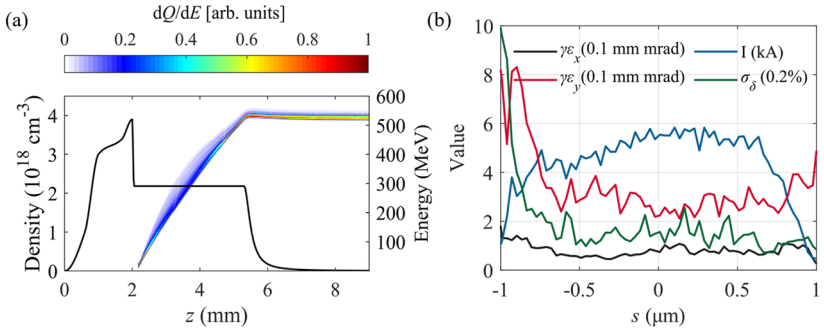

FIG. 3. PIC simulation results for LWFA. (a) Density profile used in the simulation and corresponding evolution of the energy spectrum dQ/dE of the e beam as a function of the longitudinal positions, where Q and E are the beam charge and energy, respectively. (b) Normalized emittance in the horizontal (black) and vertical (red) directions, beam current (blue), and relative energy spreads (RES) over slices. Each slice has a length of 31.25 nm, which is chosen as the grid size in the PIC simulation.

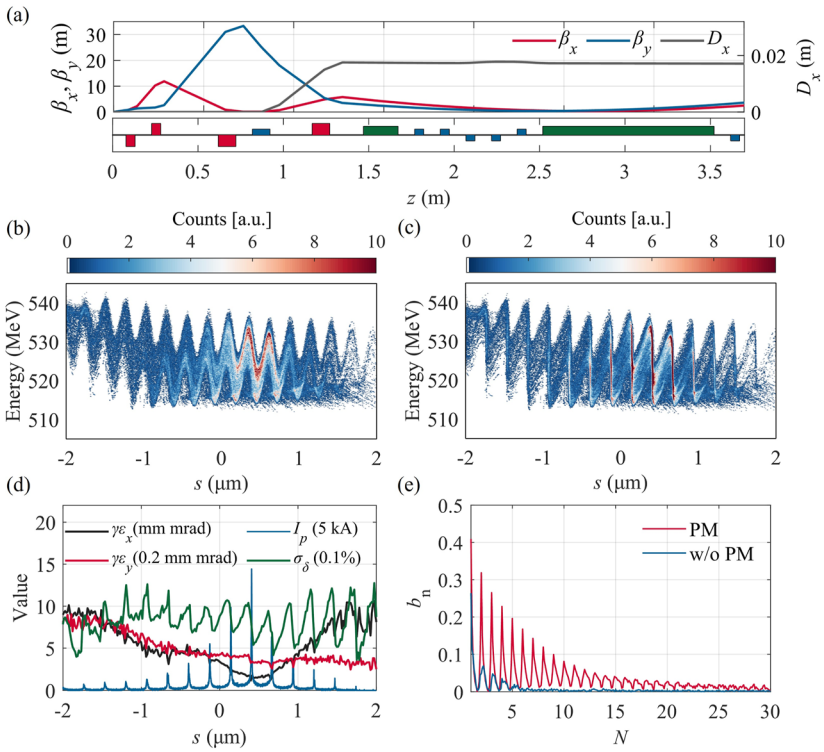

FIG. 4. Phase merging with the normal dispersion scheme. (a) Evolution of the Twiss parameters β_x and β_y and horizontal dispersion D_x along the beamline and the corresponding schematic layout of the beamline, with quadrupoles, dipoles, and undulators represented by red, blue, and green squares, respectively. (b) and (c) Longitudinal phase-space snapshots of the e beam at the exit of the modulator and the entrance of the radiator, respectively. (d) Normalized emittances in the horizontal (black) and vertical (red) directions, beam current (blue), and relative energy spread (RES, green) over slices. (e) Corresponding bunching factors for the phase merging (PM, red) and without phase merging (w/o PM, blue) situations, respectively.

peak power 50 GW, FWHM pulse width 30 fs, and waist radius 300 μm. The corresponding energy modulation amplitude $A = 1.3$ can be estimated from the simulation. As mentioned in Sec. II, for the tenth harmonic, the optimized coefficients induced by DS-II can be calculated as $R_{51} = 2.9 \times 10^{-4}$ and $R_{56} = -3.0 \times 10^{-6}$ m. More importantly, the coefficient R_{52} induced by DS-II should be optimized to zero to prevent the bunching being washed out. Cascading a magnet dipole and a chicane can provide this condition. The length of each dipole is 5 cm and the distance between any two adjacent dipoles is 10 cm in DS-II. The corresponding bending angles for the dipole and chicane are 0.29 and 3.36 mrad, respectively.

The longitudinal phase-space distributions of the e beam at the exit of the modulator and the entrance of the radiator are shown in Figs. 4(b) and 4(c). The interaction between the electrons and the seed laser imprints the energy modulation of the e beam at the seed wavelength in the modulator. This energy modulation transforms into an associated density modulation in the following DS-II. Figure 4(d) shows the transverse normalized emittances, the relative energy spread (RES), and the current profile before entering the radiator. The growth in emittance is mainly induced by the increase of the beam size due to the horizontal dispersion, and the current profile exhibits multiple spikes with a maximum spike of 72.1 kA in the phase merging scheme. The corresponding bunching factors are shown in Fig. 4(e). Here, the situation without phase merging is also plotted for comparison, where the bending angle of the dipole in DS-II has been set to 0 with a vanishing R_{51}. Such a high peak current and effective bunching will benefit the coherent radiation in the ultrashort (10 s periods) downstream undulator (radiator).

C. Phase merging with angular dispersion

An angular-dispersion-induced phase merging scheme has been proposed for the case of an extremely low-emittance storage ring,[27] but, with a number of modifications, it is also suitable for e beams from optimized operation LWFAs. For the angular dispersion scheme, the coefficient induced by DS-I is R_{26} and can be realized with a single dipole. The corresponding coefficients R_{52} and R_{56} can be induced by cascading a dogleg and a chicane with a vanishing R_{51}, as indicated in the Appendix [see Eq. (A4)]. The coefficients are calculated as $R_{52} = -b_d L_{\mathrm{dr}}$ and $R_{56} = b_d^2 L_{\mathrm{dr}} + 2b_c^2 L_{\mathrm{dr}}$, where b_d and b_c are the bending angles of the dogleg and the chicane, respectively, and L_{dr} is the drift length between each dipole in DS-II. Once R_{52} has been determined, R_{56} can be optimized separately.

The total beamline and the evolution of the e-beam parameters are plotted in Fig. 5(a). The beam elements are the same as in the normal dispersion scheme, except for those in DS-I and DS-II. The

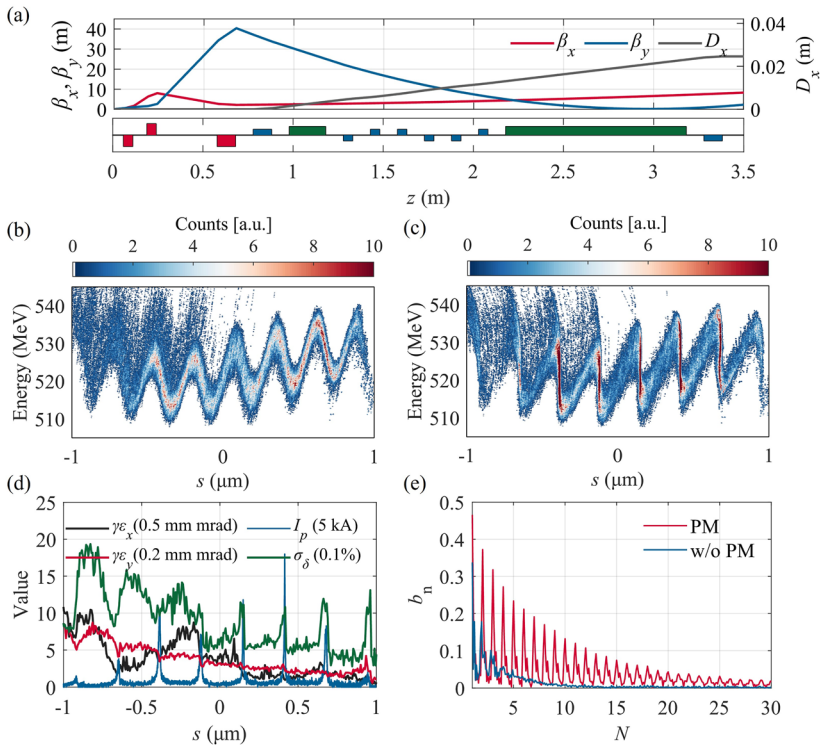

FIG. 5. Phase merging with the angular dispersion scheme. (a) Evolution of the Twiss parameters β_x and β_y and horizontal dispersion D_x along the beamline and the corresponding schematic layout of the beamline, with the quadrupoles, dipoles, and undulators represented by red, blue and green squares, respectively. (b) and (c) Longitudinal phase-space snapshots of the e beam at the exit of the modulator and the entrance of the radiator, respectively. (d) Normalized emittances in the horizontal (black) and vertical (red) directions, beam current (blue), and relative energy spreads (RES, green) over slices. (e) Corresponding bunching factors for the phase merging (PM, red) and without phase merging (w/o PM, blue) situations, respectively.

DS-I stage consists a single dipole with deflection angle 0.01 rad and length 10 cm to provide an appropriate coefficient R_{26} of 0.01. A 266 nm seed laser with peak power 100 GW, waist radius 300 μm, and pulse duration 30 fs (FWHM) interacts with the e beam in a four-period modulator with period length of 5 cm. Thus, the optimized coefficients induced by DS-II can be calculated as $R_{52} = 4.3 \times 10^{-4}$ and $R_{56} = -1.8 \times 10^{-6}$ m, with a corresponding amplitude of energy modulation of $A = 2.1$. The bending angles are thus 2.84 and 1.70 mrad for the dogleg and chicane, respectively. Figures 5(b)–5(e) show the longitudinal phase-space distributions of the e beam at the exit of the modulator and the entrance of the radiator, the beam parameters before entering the radiator, and the corresponding bunching factor. The maximum current spike reaches 89.9 kA with a bunching factor of 13.2% for the tenth harmonic, indicating the effectiveness of the angular dispersion scheme. It should be noted that the bending angle of the dogleg has been set to be 0, and the bending angle of the chicane has been adjusted accordingly to leave R_{56} unchanged for the comparison case without phase merging. As indicated in Sec. II, the angular dispersion scheme would be more efficient with an extremely low initial emittance of the e beam, which can be an alternative goal for future optimization in LWFAs.

D. Phase merging with angular modulation and dispersion

Angular modulation is an alternative option to energy modulation. It was first proposed for attosecond X-ray pulse generation with a Hermite–Gaussian TEM10 mode seeding[65] and was then applied to the CHG scheme to achieve a considerably high harmonic number.[53] This technique has been developed with the beam wavefront tilting or off-resonant laser modulation methods,[54,55] with a seed laser with fundamental Gaussian mode being used instead of the TEM10 mode. Here, we demonstrate the effective operation of bunching enhancement with an angular modulation and dispersion scheme, where the coefficient induced by DS-I is R_{12} and the corresponding coefficients in DS-II are R_{51} and R_{52}. The coefficient R_{12} indicates the coupling between the horizontal position and momentum and can be tuned by varying the strength of the quadrupoles and the position in the beamline. A dipole or a combination of a dipole and quadrupoles can provide appropriate R_{51} and R_{52}, and can be used in DS-II. It should be noted that R_{56} still remains, but it can be ignored for a small bending angle of the dipole.

The beamline and the evolution of the e-beam parameters are shown in Fig. 6(a). The coefficient R_{51} has been naturally

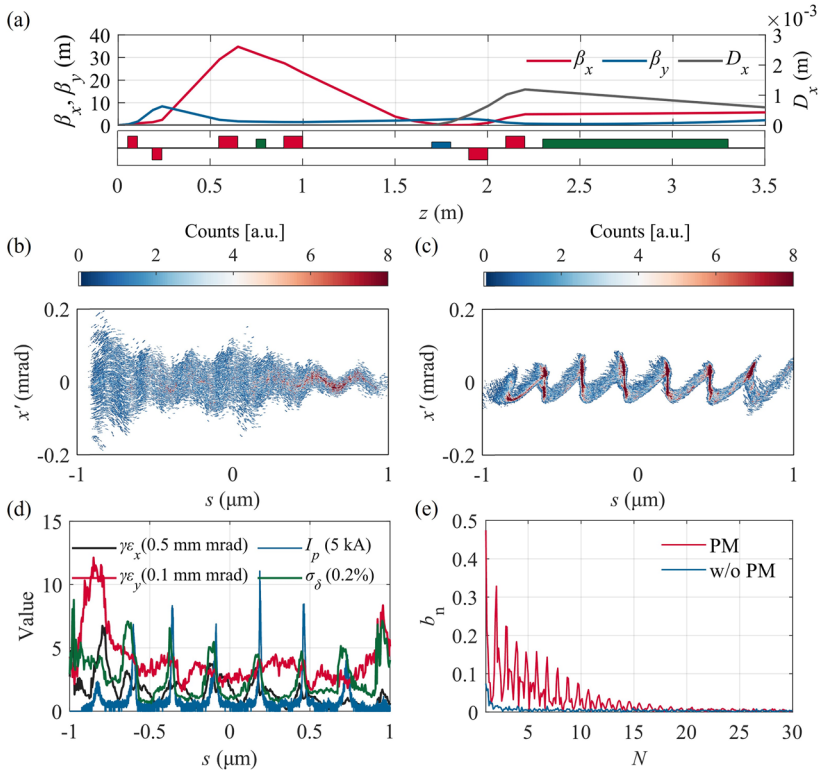

FIG. 6. Phase merging with the angular modulation and dispersion scheme. (a) Evolution of the Twiss parameters β_x and β_y and horizontal dispersion D_x along the beamline and the corresponding schematic layout of the beamline, with the quadrupoles, dipoles, and undulators represented by red, blue and green squares, respectively. (b) and (c) Longitudinal phase-space snapshots of the *e* beam at the exit of the modulator and the entrance of the radiator, respectively. (d) Normalized emittances in the horizontal (black) and vertical (red) directions, beam current (blue), and relative energy spreads (RES, green) over slices. (e) Corresponding bunching factors for the phase merging (PM, red) and without phase merging (w/o PM, blue) situations, respectively.

induced during the focusing stage, and the angular modulation has been imprinted with an off-resonant laser modulation technique. A 266 nm seed laser with peak power 2 TW interacts with the *e* beam in the one-period modulator with period length 5 cm and resonant wavelength 133 nm. The corresponding angular modulation amplitude is estimated to be $A = 0.4$. Appropriate coupling coefficients R_{51} and R_{52} are then estimated to be $R_{51} = 1.8 \times 10^{-3}$ and $R_{52} = 3.1 \times 10^{-3}$ m, with corresponding quadrupole strengths k of 6.2 m^{-2} and a bending angle of 3.5 mrad for the dipole in DS-II. The subsequent two quadrupoles are applied to ensure effective focusing of the *e* beam and have less effect on the bunching. The remaining coefficient R_{56} equals 2.0×10^{-7} m, which makes no contribution to the bunching and can be ignored. The s–x' phase-space distributions of the *e* beam at the exit of the modulator and the entrance of the radiator, along with the beam parameters and the corresponding bunching factors, are shown in Figs. 6(b)–6(e). The maximum peak current reaches 55.3 kA, which is lower than in the aforementioned two schemes. Further optimization of the initial beam emittance will be beneficial for such a scheme with a higher bunching efficiency. A summary of the main parameters and results for the three configurations is presented in Table I.

E. LWFA-driven coherent harmonic generation

Here, we take the phase merging scheme with angular dispersion as an example to show the effectiveness of the proposed scheme and the properties of the radiation. The micro-bunched *e* beam is sent to a 2 cm-period-length radiator with 50 periods. The radiation performance for such pre-bunched *e* beam is simulated and studied using the 3D non-period-averaged simulation tool Mithra-2.0,[66] as shown in Fig. 7. The radiation energy reaches 2.4 μJ at the exit of the 50-period radiator [see Fig. 7(a)]. The radiation starts from the initial bunching of the *e* beam exhibiting multiple spikes, and then a single spike dominates with a peak power of 0.43 GW for 15 radiator periods, as shown by the blue line in Fig. 7(b). As the period number increases, the former spike slips forward relative to the bunch, and new spikes form. The duration of the radiation thus gets longer and several spikes appear, as shown by the green and red lines in Fig. 7(b). The corresponding spectrum at the exit of the radiator is

TABLE I. Simulated parameters and results for the three configurations.

Parameters	Phase merging with normal dispersion	Phase merging with angular dispersion	Phase merging with angular modulation and dispersion
DS-I	Dipole	Dipole	Quadrupoles and drift
Key transport matrix components in DS I	R_{16} = 1.75 cm	R_{26} = 0.01	R_{12} (varies along beamline)
DS-II	Dipole and chicane	Dogleg and chicane	Dipole
Key transport matrix components in DS II	$R_{51} = 2.9 \times 10^{-4}$ $R_{56} = -3.0 \times 10^{-6}$ m	$R_{52} = 4.3 \times 10^{-4}$ m $R_{56} = -1.8 \times 10^{-6}$ m	$R_{51} = 1.8 \times 10^{-4}$ $R_{52} = 3.1 \times 10^{-3}$ m
Seed wavelength	266 nm	266 nm	266 nm
Power of seed laser	50 GW	100 GW	2 TW
Pulse width (FWHM)	30 fs	30 fs	30 fs
Waist radius	300 μm	300 μm	300 μm
Peak current	72.1 kA	89.9 kA	55.3 kA
Bunching factor (tenth)	8.1%	13.2%	3.1%

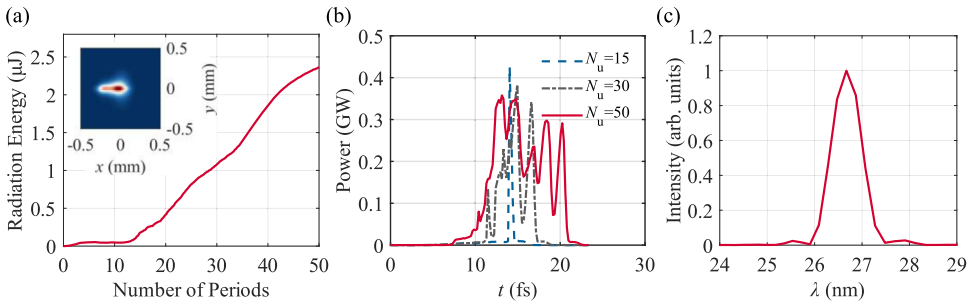

FIG. 7. Radiation properties of phase merging scheme with angular dispersion. (a) Radiation energy along the periods of the radiator and corresponding transverse profile of radiation at the exit of the radiator. (b) Power profile of radiation for various periods of the radiator. (c) Spectrum at the exit of the radiator.

shown in Fig. 7(c). The peak brilliance of the radiation is estimated to be 1.41×10^{29} photons s^{-1} mm^{-1} $mrad^{-1}$ (0.1% BW)$^{-1}$.

IV. DISCUSSION

The effective operation of the bunching enhanced scheme with phase merging effects has been illustrated for various configurations with e beams from LWFAs, including normal dispersion, angular dispersion, and the angular modulation and dispersion schemes. The corresponding bunching factor for such schemes is described by Eq. (4). Compared with the normal CHG scheme, the quantity σ_i/R_{ij} (i, j = 1, 2, 6 and $i < j$) takes the place of σ_δ in the exponential attenuation term. Full advantage can be taken of this, with an extremely small σ_i/R_{ij} being optimized to slow down the decrease in bunching

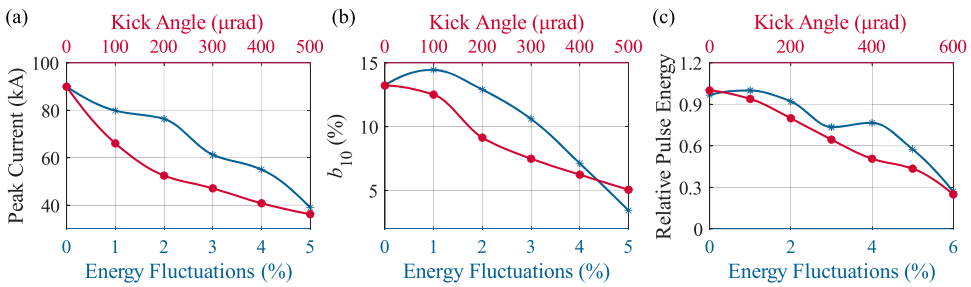

FIG. 8. Tolerances of the presented angular dispersion scheme with regard to energy fluctuations and pointing jitter. (a) Peak current, (b) bunching factor for the tenth harmonic, and (c) relative pulse energy as functions of energy fluctuations and pointing jitter at the beamline entrance (the exit of the plasma).

factor with increasing harmonic number. For the presented angular dispersion scheme, σ_i/R_{ij} evolves to σ_2/R_{26} and thus can be estimated as 1.18×10^{-3}, which is obviously lower than the relative energy spread σ_δ of order 1% and even the relative energy spread over slices of ~0.34%, as indicated in Fig. 3(b). The term σ_2/R_{26} can be regarded as the local (effective) energy spread or energy spread over energy slices, which is much lower than the global one.[67,68] This is the key aspect of the bunching enhanced scheme with phase merging effects.

There are still several physical issues that need to be considered for practical applications with *e* beams from LWFAs. We discuss these briefly and demonstrate the feasibility of the proposed scheme by evaluating the tolerances of the bunching, the peak current, and the relative pulse energy with regard to *e*-beam energy fluctuations and pointing jitters. The tolerance of the point jitter is evaluated by imposing artificially induced kicks at the beginning of the beamline (the exit of the plasma). It should be noted that the kick angle is added in both the horizontal and vertical directions simultaneously. Figure 8 shows the peak current, the bunching factor for the tenth harmonic, and the relative pulse energy as functions of the initial energy fluctuations and kick angles. In general, the peak current, the bunching factor, and the pulse energy all decrease in the presence of initial energy fluctuations or kicks, mainly as a result of the deviation from the optimized conditions and the weak modulation due to the spatial separation between the *e* beam and the seed laser. However, ~30% of the radiation energy is still attainable even with a large energy fluctuation of up to 6% or a kick error of up to 0.6 mrad, as indicated in Fig. 8(c). The presented scheme thus offers new opportunities for LWFA-driven high-gain FELs with robust operation, which can be achieved with the experimental parameters reported in Ref. 47.

V. CONCLUSION

We have proposed bunching enhanced schemes for coherent radiation by using phase merging effects with a DS-M-DS configuration. Benefitting from the specific phase-space coupling of the beam induced by DS-I, the electrons in the modulated beam can merge to the same phase within one seed wavelength with a matching DS-II, leading to a significant increase in up-conversion efficiency. Taking *e* beams from LWFAs as examples, we have demonstrated effective operation of the proposed schemes through start-to-end simulations, including schemes with normal dispersion, angular dispersion, and angular modulation and dispersion configurations. The radiation properties have been investigated for the angular dispersion scheme, which has a total beamline within 3.5 m and an output pulse energy of 2.4 μJ for the tenth harmonic with a seeding wavelength of 266 nm. The robustness of the proposed schemes has also been investigated through the artificial addition of fluctuations or kicks on the *e* beam at the beginning of the beamline, and acceptable tolerances have been found even for large energy fluctuations and kicks of up to 6% and 0.6 mrad, respectively. The proposed schemes offer new opportunities for high-gain FELs driven by LWFAs with robust operation and provide a basis for future optimization and design of compact FELs. Furthermore, they generalize the operation of PEHG schemes[26] and can be applied to a variety of *e*-beam sources with different properties.

ACKNOWLEDGMENTS

This work was supported by the National Natural Science Foundation of China (Grant Nos. 12388102, 12225411, 12105353, 11991072, and 12174410), the CAS Project for Young Scientists in Basic Research (Grant No. YSBR060), the Program of Shanghai Academic Research Leader (Grant No. 22XD1424200), and the State Key Laboratory Program of the Chinese Ministry of Science and Technology and CAS Youth Innovation Promotion Association (Y201952 and 2022242).

AUTHOR DECLARATIONS

Conflict of Interest

The authors have no conflicts to disclose.

Author Contributions

Ke Feng: Conceptualization (lead); Data curation (lead); Formal analysis (lead); Investigation (lead); Methodology (lead); Visualization (lead); Writing – original draft (lead); Writing – review & editing (equal). **Kangnan Jiang**: Conceptualization (equal); Formal analysis (equal). **Runshu Hu**: Conceptualization (equal); Methodology (equal). **Shixia Luan**: Conceptualization (equal). **Wentao Wang**: Formal analysis (equal); Supervision (equal); Writing – review & editing (equal). **Ruxin Li**: Supervision (equal).

DATA AVAILABILITY

The data that support the findings of this study are available from the corresponding authors upon reasonable request.

APPENDIX: Transfer Matrix for dispersion section

In this Appendix, we provide a simple description of the design of the dispersion section using the transfer-matrix method. Here, we omit (y, y') for simplicity, i.e., (x, x', z, δ) is used in the following analysis. The transfer matrices for a thin-lens magnet dipole and the chicane can be described as follows:

$$M_{\text{dipole}} = \begin{pmatrix} 1 & 0 & 0 & 0 \\ 0 & 1 & 0 & -b \\ b & 0 & 1 & 0 \\ 0 & 0 & 0 & 1 \end{pmatrix}, \quad M_{\text{chicane}} = \begin{pmatrix} 1 & 3L_c & 0 & 0 \\ 0 & 1 & 0 & 0 \\ 0 & 0 & 1 & 2b_c^2 L_c \\ 0 & 0 & 0 & 1 \end{pmatrix}, \tag{A1}$$

where b is the bending angle of the dipole, and b_c and L_c are the bending angle and the distance between each dipole in the chicane. The total transfer matrix for cascading a dipole and a chicane can be expressed as follows:

$$\begin{aligned} M_{\text{dipole}-\text{chicane}} &= M_{\text{chicane}} M_{\text{drift}} M_{\text{dipole}} \\ &= \begin{pmatrix} 1 & 3L_c + L_{\text{dr}} & 0 & -b(3L_c + L_{\text{dr}}) \\ 0 & 1 & 0 & -b \\ b & 0 & 1 & 2b_c^2 L_c \\ 0 & 0 & 0 & 1 \end{pmatrix}, \end{aligned} \tag{A2}$$

where L_{dr} is the drift length between the dipole and the chicane. The total transfer matrix has the required coupling coefficients $R_{51} = b$ and $R_{56} = 2b_c^2 L_c$, which can be separately adjusted and applied in the phase merging scheme with normal dispersion.

For phase merging with the angular dispersion scheme, the coefficient R_{52} is needed and can be provided by a dogleg with corresponding transfer matrix

$$M_{\text{dogleg}} = \begin{pmatrix} 1 & L_d & 0 & -b_d L_d \\ 0 & 1 & 0 & 0 \\ 0 & -b_d L_d & 1 & b_d^2 L_d \\ 0 & 0 & 0 & 1 \end{pmatrix}, \tag{A3}$$

where b_d and L_d are the bending angle and distance between the dipoles in the dogleg. Although the coupling coefficients R_{52} and R_{56} can be maintained simultaneously with a vanishing R_{51}, these two coefficients are coupled with each other, and this leads to poor scalability for various parameters. Cascading a dogleg and a chicane provides an additional term in R_{56}, which is independent from the dogleg, and this approach is more feasible for various situations. The corresponding transfer matrix can be expressed as

$$\begin{aligned} M_{\text{dogleg}-\text{chicane}} &= M_{\text{chicane}} M_{\text{drift}} M_{\text{dogleg}} \\ &= \begin{pmatrix} 1 & 5L_D & 0 & -b_d L_D \\ 0 & 1 & 0 & 0 \\ 0 & -b_d L_D & 1 & b_d^2 L_D + 2b_c^2 L_D \\ 0 & 0 & 0 & 1 \end{pmatrix}, \end{aligned} \tag{A4}$$

where the distance between each two dipoles is assumed to be L_D in the dogleg–chicane cascading configuration.

For the phase merging with angular modulation and dispersion scheme, the coefficients R_{51} can be induced with a dipole, as indicated by Eq. (A1). Along with an appropriate drift section, the dipole can provide a coupling coefficient R_{52} to achieve phase merging. An inserted quadrupole makes DS-II more feasible, and the corresponding transfer matrix for DS-II can be expressed as

$$\begin{aligned} M_{\text{quadruple}-\text{dipole}} &= M_{\text{dipole}} M_{\text{drift}} M_{\text{quadruple}} \\ &= \begin{pmatrix} 1 - kL_q L_{\text{dr}} & L_q + L_{\text{dr}} & 0 & 0 \\ -kL_q & 1 & 0 & -b \\ b(1 - kL_q L_{\text{dr}}) & b(L + L_{\text{dr}}) & 1 & 0 \\ 0 & 0 & 0 & 1 \end{pmatrix}, \end{aligned} \tag{A5}$$

where k and L_q are the focusing strength and the length of the quadrupole.

Equations (A2), (A4), and (A5) provide the design principles for DS-II in the cases of phase merging schemes with normal dispersion, angular dispersion, and angular modulation and dispersion, respectively. The specific parameters and designs are discussed in Sec. III.

REFERENCES

[1] J. M. J. Madey, "Stimulated emission of bremsstrahlung in a periodic magnetic field," J. Appl. Phys. **42**, 1906–1913 (1971).

[2] C. Bostedt, S. Boutet, D. M. Fritz, Z. R. Huang, H. J. Lee, H. T. Lemke, A. Robert, W. F. Schlotter, J. J. Turner, and G. J. Williams, "Linac coherent light source: The first five years," Rev. Mod. Phys. **88**, 015007 (2016).

[3] P. Emma, R. Akre, J. Arthur, R. Bionta, C. Bostedt, J. Bozek, A. Brachmann, P. Bucksbaum, R. Coffee, F. J. Decker, Y. Ding, D. Dowell, S. Edstrom, A. Fisher, J. Frisch, S. Gilevich, J. Hastings, G. Hays, P. Hering, Z. Huang, R. Iverson, H. Loos, M. Messerschmidt, A. Miahnahri, S. Moeller, H. D. Nuhn, G. Pile, D. Ratner, J. Rzepiela, D. Schultz, T. Smith, P. Stefan, H. Tompkins, J. Turner, J. Welch, W. White, J. Wu, G. Yocky, and J. Galayda, "First lasing and operation of an angstrom-wavelength free-electron laser," Nat. Photonics **4**, 641–647 (2010).

[4] T. Ishikawa, H. Aoyagi, T. Asaka, Y. Asano, N. Azumi, T. Bizen, H. Ego, K. Fukami, T. Fukui, Y. Furukawa, S. Goto, H. Hanaki, T. Hara, T. Hasegawa, T. Hatsui, A. Higashiya, T. Hirono, N. Hosoda, M. Ishii, T. Inagaki, Y. Inubushi, T. Itoga, Y. Joti, M. Kago, T. Kameshima, H. Kimura, Y. Kirihara, A. Kiyomichi, T. Kobayashi, C. Kondo, T. Kudo, H. Maesaka, X. M. Marechal, T. Masuda, S. Matsubara, T. Matsumoto, T. Matsushita, S. Matsui, M. Nagasono, N. Nariyama, H. Ohashi, T. Ohata, T. Ohshima, S. Ono, Y. Otake, C. Saji, T. Sakurai, T. Sato, K. Sawada, T. Seike, K. Shirasawa, T. Sugimoto, S. Suzuki, S. Takahashi, H. Takebe, K. Takeshita, K. Tamasaku, H. Tanaka, R. Tanaka, T. Tanaka, T. Togashi, K. Togawa, A. Tokuhisa, H. Tomizawa, K. Tono, S. K. Wu, M. Yabashi, M. Yamaga, A. Yamashita, K. Yanagida, C. Zhang, T. Shintake, H. Kitamura, and N. Kumagai, "A compact X-ray free-electron laser emitting in the sub-angstrom region," Nat. Photonics **6**, 540–544 (2012).

[5] H. S. Kang, C. K. Min, H. Heo, C. Kim, H. Yang, G. Kim, I. Nam, S. Y. Baek, H. J. Choi, G. Mun, B. R. Park, Y. J. Suh, D. C. Shin, J. Hu, J. Hong, S. Jung, S. H. Kim, K. Kim, D. Na, S. S. Park, Y. J. Park, J. H. Han, Y. G. Jung, S. H. Jeong, H. G. Lee, S. Lee, S. Lee, W. W. Lee, B. Oh, H. S. Suh, Y. W. Parc, S. J. Park, M. H. Kim, N. S. Jung, Y. C. Kim, M. S. Lee, B. H. Lee, C. W. Sung, I. S. Mok, J. M. Yang, C. S. Lee, H. Shin, J. H. Kim, Y. Kim, J. H. Lee, S. Y. Park, J. Kim, J. Park, I. Eom, S. Rah, S. Kim, K. H. Nam, J. Park, J. Park, S. Kim, S. Kwon, S. H. Park, K. S. Kim, H. Hyun, S. N. Kim, S. Kim, S. M. Hwang, M. J. Kim, C. Y. Lim, C. J. Yu, B. S. Kim, T. H. Kang, K. W. Kim, S. H. Kim, H. S. Lee, H. S. Lee, K. H. Park, T. Y. Koo, D. E. Kim, and I. S. Ko, "Hard X-ray free-electron laser with femtosecond-scale timing jitter," Nat. Photonics **11**, 708–713 (2017).

[6] W. Decking, S. Abeghyan, P. Abramian *et al.*, "A MHz-repetition-rate hard X-ray free-electron laser driven by a superconducting linear accelerator," Nat. Photonics **14**, 391–397 (2020).

[7] Z. R. Huang and K. J. Kim, "Review of x-ray free-electron laser theory," Phys. Rev. Spec. Top.–Accel. Beams **10**, 034801 (2007).

[8] C. Pellegrini, A. Marinelli, and S. Reiche, "The physics of x-ray free-electron lasers," Rev. Mod. Phys. **88**, 015006 (2016).

[9] C. Feng and H. X. Deng, "Review of fully coherent free-electron lasers," Nucl. Sci. Tech. **29**, 160 (2018).

[10] A. Gover, R. Ianconescu, A. Friedman, C. Emma, N. Sudar, P. Musumeci, and C. Pellegrini, "Superradiant and stimulated-superradiant emission of bunched electron beams," Rev. Mod. Phys. **91**, 035003 (2019).

[11] N. Sudar, P. Musumeci, J. Duris, I. Gadjev, M. Polyanskiy, I. Pogorelsky, M. Fedurin, C. Swinson, K. Kusche, M. Babzien, and A. Gover, "High efficiency energy extraction from a relativistic electron beam in a strongly tapered undulator," Phys. Rev. Lett. **117**, 174801 (2016).

[12] C. Emma, N. Sudar, P. Musumeci, A. Urbanowicz, and C. Pellegrini, "High efficiency tapered free-electron lasers with a prebunched electron beam," Phys. Rev. Accel. Beams **20**, 110701 (2017).

[13] L. H. Yu, "Generation of intense uv radiation by subharmonically seeded single-pass free-electron lasers," Phys. Rev. A **44**, 5178–5193 (1991).

[14] L. H. Yu, M. Babzien, I. Ben-Zvi, L. F. DiMauro, A. Doyuran, W. Graves, E. Johnson, S. Krinsky, R. Malone, I. Pogorelsky, J. Skaritka, G. Rakowsky, L. Solomon, X. J. Wang, M. Woodle, V. Yakimenko, S. G. Biedron, J. N. Galayda, E. Gluskin, J. Jagger, V. Sajaev, and I. Vasserman, "High-gain harmonic-generation free-electron laser," Science **289**, 932–934 (2000).

[15] E. Allaria, R. Appio, L. Badano, W. A. Barletta, S. Bassanese, S. G. Biedron, A. Borga, E. Busetto, D. Castronovo, P. Cinquegrana, S. Cleva, D. Cocco, M. Cornacchia, P. Craievich, I. Cudin, G. D'Auria, M. Dal Forno, M. B. Danailov, R. De Monte, G. De Ninno, P. Delgiusto, A. Demidovich, S. Di Mitri, B. Diviacco, A. Fabris, R. Fabris, W. Fawley, M. Ferianis, E. Ferrari, S. Ferry, L. Froehlich, P. Furlan, G. Gaio, F. Gelmetti, L. Giannessi, M. Giannini, R. Gobessi, R. Ivanov,

E. Karantzoulis, M. Lonza, A. Lutman, B. Mahieu, M. Milloch, S. V. Milton, M. Musardo, I. Nikolov, S. Noe, F. Parmigiani, G. Penco, M. Petronio, L. Pivetta, M. Predonzani, F. Rossi, L. Rumiz, A. Salom, C. Scafuri, C. Serpico, P. Sigalotti, S. Spampinati, C. Spezzani, M. Svandrlik, C. Svetina, S. Tazzari, M. Trovo, R. Umer, A. Vascotto, M. Veronese, R. Visintini, M. Zaccaria, D. Zangrando, and M. Zangrando, "Highly coherent and stable pulses from the FERMI seeded free-electron laser in the extreme ultraviolet," Nat. Photonics **6**, 699–704 (2012).

[16]B. Girard, Y. Lapierre, J. M. Ortega, C. Bazin, M. Billardon, P. Elleaume, M. Bergher, M. Velghe, and Y. Petroff, "Optical frequency multiplication by an optical klystron," Phys. Rev. Lett. **53**, 2405–2408 (1984).

[17]M. Labat, M. Hosaka, A. Mochihashi, M. Shimada, M. Katoh, G. Lambert, T. Hara, Y. Takashima, and M. E. Couprie, "Coherent harmonic generation on UVSOR-II storage ring," Eur. Phys. J. D **44**, 187–200 (2007).

[18]E. Hemsing, G. Stupakov, D. Xiang, and A. Zholents, "Beam by design: Laser manipulation of electrons in modern accelerators," Rev. Mod. Phys. **86**, 897–941 (2014).

[19]L. H. Yu and I. BenZvi, "High-gain harmonic generation of soft X-rays with the 'fresh bunch' technique," Nucl. Instrum. Methods Phys. Res., Sect. A **393**, 96–99 (1997).

[20]E. Allaria, D. Castronovo, P. Cinquegrana, P. Craievich, M. Dal Forno, M. B. Danailov, G. D'Auria, A. Demidovich, G. De Ninno, S. Di Mitri, B. Diviacco, W. M. Fawley, M. Ferianis, E. Ferrari, L. Froehlich, G. Gaio, D. Gauthier, L. Giannessi, R. Ivanov, B. Mahieu, N. Mahne, I. Nikolov, F. Parmigiani, G. Penco, L. Raimondi, C. Scafuri, C. Serpico, P. Sigalotti, S. Spampinati, C. Spezzani, M. Svandrlik, C. Svetina, M. Trovo, M. Veronese, D. Zangrando, and M. Zangrando, "Two-stage seeded soft-X-ray free-electron laser," Nat. Photonics **7**, 913–918 (2013).

[21]G. Stupakov, "Using the beam-echo effect for generation of short-wavelength radiation," Phys. Rev. Lett. **102**, 074801 (2009).

[22]D. Xiang, E. Colby, M. Dunning, S. Gilevich, C. Hast, K. Jobe, D. McCormick, J. Nelson, T. O. Raubenheimer, K. Soong, G. Stupakov, Z. Szalata, D. Walz, S. Weathersby, M. Woodley, and P. L. Pernet, "Demonstration of the echo-enabled harmonic generation technique for short-wavelength seeded free electron lasers," Phys. Rev. Lett. **105**, 114801 (2010).

[23]Z. T. Zhao, D. Wang, J. H. Chen, Z. H. Chen, H. X. Deng, J. G. Ding, C. Feng, Q. Gu, M. M. Huang, T. H. Lan, Y. B. Leng, D. G. Li, G. Q. Lin, B. Liu, E. Prat, X. T. Wang, Z. S. Wang, K. R. Ye, L. Y. Yu, H. O. Zhang, J. Q. Zhang, M. Zhang, M. Zhang, T. Zhang, S. P. Zhong, and Q. G. Zhou, "First lasing of an echo-enabled harmonic generation free-electron laser," Nat. Photonics **6**, 360–363 (2012).

[24]E. Hemsing, M. Dunning, B. Garcia, C. Hast, T. Raubenheimer, G. Stupakov, and D. Xiang, "Echo-enabled harmonics up to the 75th order from precisely tailored electron beams," Nat. Photonics **10**, 512–515 (2016).

[25]P. Rebernik Ribič, A. Abrami, L. Badano, M. Bossi, H. H. Braun, N. Bruchon, F. Capotondi, D. Castronovo, M. Cautero, P. Cinquegrana, M. Coreno, M. E. Couprie, I. Cudin, M. Boyanov Danailov, G. De Ninno, A. Demidovich, S. Di Mitri, B. Diviacco, W. M. Fawley, C. Feng, M. Ferianis, E. Ferrari, L. Foglia, F. Frassetto, G. Gaio, D. Garzella, A. Ghaith, F. Giacuzzo, L. Giannessi, V. Grattoni, S. Grulja, E. Hemsing, F. Iazzourene, G. Kurdi, M. Lonza, N. Mahne, M. Malvestuto, M. Manfredda, C. Masciovecchio, P. Miotti, N. S. Mirian, I. Petrov Nikolov, G. M. Penco, G. Penn, L. Poletto, M. Pop, E. Prat, E. Principi, L. Raimondi, S. Reiche, E. Roussel, R. Sauro, C. Scafuri, P. Sigalotti, S. Spampinati, C. Spezzani, L. Sturari, M. Svandrlik, T. Tanikawa, M. Trovo, M. Veronese, D. Vivoda, D. Xiang, M. Zaccaria, D. Zangrando, M. Zangrando, and E. M. Allaria, "Coherent soft X-ray pulses from an echo-enabled harmonic generation free-electron laser," Nat. Photonics **13**, 555–561 (2019).

[26]C. Feng, H. X. Deng, D. Wang, and Z. T. Zhao, "Phase-merging enhanced harmonic generation free-electron laser," New J. Phys. **16**, 043021 (2014).

[27]C. Feng and Z. T. Zhao, "A storage ring based free-electron laser for generating ultrashort coherent EUV and X-ray radiation," Sci. Rep. **7**, 4724 (2017).

[28]C. L. Li, C. Feng, and B. C. Jiang, "Extremely bright coherent synchrotron radiation production in a diffraction-limited storage ring using an angular dispersion-induced microbunching scheme," Phys. Rev. Accel. Beams **23**, 110701 (2020).

[29]T. Tajima and J. M. Dawson, "Laser electron accelerator," Phys. Rev. Lett. **43**, 267–270 (1979).

[30]K. Nakajima, D. Fisher, T. Kawakubo, H. Nakanishi, A. Ogata, Y. Kato, Y. Kitagawa, R. Kodama, K. Mima, H. Shiraga, K. Suzuki, K. Yamakawa, T. Zhang, Y. Sakawa, T. Shoji, Y. Nishida, N. Yugami, M. Downer, and T. Tajima, "Observation of ultrahigh gradient electron acceleration by a self-modulated intense short laser pulse," Phys. Rev. Lett. **74**, 4428–4431 (1995).

[31]E. Esarey, C. B. Schroeder, and W. P. Leemans, "Physics of laser-driven plasma-based electron accelerators," Rev. Mod. Phys. **81**, 1229 (2009).

[32]J. Faure, Y. Glinec, A. Pukhov, S. Kiselev, S. Gordienko, E. Lefebvre, J. P. Rousseau, F. Burgy, and V. Malka, "A laser-plasma accelerator producing monoenergetic electron beams," Nature **431**, 541–544 (2004).

[33]C. G. R. Geddes, C. Toth, J. van Tilborg, E. Esarey, C. B. Schroeder, D. Bruhwiler, C. Nieter, J. Cary, and W. P. Leemans, "High-quality electron beams from a laser wakefield accelerator using plasma-channel guiding," Nature **431**, 538–541 (2004).

[34]S. P. D. Mangles, C. D. Murphy, Z. Najmudin, A. G. R. Thomas, J. L. Collier, A. E. Dangor, E. J. Divall, P. S. Foster, J. G. Gallacher, C. J. Hooker, D. A. Jaroszynski, A. J. Langley, W. B. Mori, P. A. Norreys, F. S. Tsung, R. Viskup, B. R. Walton, and K. Krushelnick, "Monoenergetic beams of relativistic electrons from intense laser-plasma interactions," Nature **431**, 535–538 (2004).

[35]H. P. Schlenvoigt, K. Haupt, A. Debus, F. Budde, O. Jackel, S. Pfotenhauer, H. Schwoerer, E. Rohwer, J. G. Gallacher, E. Brunetti, R. P. Shanks, S. M. Wiggins, and D. A. Jaroszynski, "A compact synchrotron radiation source driven by a laser-plasma wakefield accelerator," Nat. Phys. **4**, 130–133 (2008).

[36]M. Fuchs, R. Weingartner, A. Popp, Z. Major, S. Becker, J. Osterhoff, I. Cortrie, B. Zeitler, R. Horlein, G. D. Tsakiris, U. Schramm, T. P. Rowlands-Rees, S. M. Hooker, D. Habs, F. Krausz, S. Karsch, and F. Gruner, "Laser-driven soft-X-ray undulator source," Nat. Phys. **5**, 826–829 (2009).

[37]T. Andre, I. A. Andriyash, A. Loulergue, M. Labat, E. Roussel, A. Ghaith, M. Khojoyan, C. Thaury, M. Valleau, F. Briquez, F. Marteau, K. Tavakoli, P. N'Gotta, Y. Dietrich, G. Lambert, V. Malka, C. Benabderrahmane, J. Veteran, L. Chapuis, T. El Ajjouri, M. Sebdaoui, N. Hubert, O. Marcouille, P. Berteaud, N. Leclercq, M. El Ajjouri, P. Rommeluere, F. Bouvet, J. P. Duval, C. Kitegi, F. Blache, B. Mahieu, S. Corde, J. Gautier, K. Ta Phuoc, J. P. Goddet, A. Lestrade, C. Herbeaux, C. Evain, C. Szwaj, S. Bielawski, A. Tafzi, P. Rousseau, S. Smartsev, F. Polack, D. Dennetiere, C. Bourassin-Bouchet, C. De Oliveira, and M. E. Couprie, "Control of laser plasma accelerated electrons for light sources," Nat. Commun. **9**, 1334 (2018).

[38]J. Faure, "Plasma injection schemes for laser–plasma accelerators," CERN Yellow Rep. **1**, 143 (2016).

[39]A. J. Gonsalves, K. Nakamura, J. Daniels, C. Benedetti, C. Pieronek, T. C. H. de Raadt, S. Steinke, J. H. Bin, S. S. Bulanov, J. van Tilborg, C. G. R. Geddes, C. B. Schroeder, C. Toth, E. Esarey, K. Swanson, L. Fan-Chiang, G. Bagdasarov, N. Bobrova, V. Gasilov, G. Korn, P. Sasorov, and W. P. Leemans, "Petawatt laser guiding and electron beam acceleration to 8 GeV in a laser-heated capillary discharge waveguide," Phys. Rev. Lett. **122**, 084081 (2019).

[40]S. Barber, J. van Tilborg, C. Schroeder, R. Lehe, H.-E. Tsai, K. Swanson, S. Steinke, K. Nakamura, C. Geddes, C. Benedetti *et al.*, "Measured emittance dependence on the injection method in laser plasma accelerators," Phys. Rev. Lett. **119**, 104801 (2017).

[41]K. Jiang, K. Feng, H. Wang, X. Yang, P. Bai, Y. Xu, Y. Leng, W. Wang, and R. Li, "Measurement of electron beam transverse slice emittance using a focused beamline," High Power Laser Sci. Eng. **11**, e36 (2023).

[42]W. T. Wang, W. T. Li, J. S. Liu, Z. J. Zhang, R. Qi, C. H. Yu, J. Q. Liu, M. Fang, Z. Y. Qin, C. Wang, Y. Xu, F. X. Wu, Y. X. Leng, R. X. Li, and Z. Z. Xu, "High-brightness high-energy electron beams from a laser wakefield accelerator via energy chirp control," Phys. Rev. Lett. **117**, 124801 (2016).

[43]L. T. Ke, K. Feng, W. T. Wang, Z. Y. Qin, C. H. Yu, Y. Wu, Y. Chen, R. Qi, Z. J. Zhang, Y. Xu, X. J. Yang, Y. X. Leng, J. S. Liu, R. X. Li, and Z. Z. Xu, "Near-GeV electron beams at a few per-mille level from a laser wakefield accelerator via density-tailored plasma," Phys. Rev. Lett. **126**, 214801 (2021).

[44]J. P. Couperus, R. Pausch, A. Kohler, O. Zarini, J. M. Kramer, M. Garten, A. Huebl, R. Gebhardt, U. Helbig, S. Bock, K. Zeil, A. Debus, M. Bussmann, U. Schramm, and A. Irman, "Demonstration of a beam loaded nanocoulombclass laser wakefield accelerator," Nat. Commun. **8**, 487 (2017).

[45]J. Gotzfried, A. Dopp, M. F. Gilljohann, F. M. Foerster, H. Ding, S. Schindler, G. Schilling, A. Buck, L. Veisz, and S. Karsch, "Physics of high-charge electron beams in laser-plasma wakefields," Phys. Rev. X **10**, 041015 (2020).

[46]A. R. Maier, N. M. Delbos, T. Eichner, L. Hubner, S. Jalas, L. Jeppe, S. W. Jolly, M. Kirchen, V. Leroux, P. Messner, M. Schnepp, M. Trunk, P. A. Walker,

C. Werle, and P. Winkler, "Decoding sources of energy variability in a laser-plasma accelerator," Phys. Rev. X **10**, 031039 (2020).
[47]W. T. Wang, K. Feng, L. T. Ke, C. H. Yu, Y. Xu, R. Qi, Y. Chen, Z. Y. Qin, Z. J. Zhang, M. Fang, J. Q. Liu, K. N. Jiang, H. Wang, C. Wang, X. J. Yang, F. X. Wu, Y. X. Leng, J. S. Liu, R. X. Li, and Z. Z. Xu, "Free-electron lasing at 27 nanometres based on a laser wakefield accelerator," Nature **595**, 516–520 (2021).
[48]M. Labat, J. C. Cabadağ, A. Ghaith, A. Irman, A. Berlioux, P. Berteaud, F. Blache, S. Bock, F. Bouvet, F. Briquez, Y. Y. Chang, S. Corde, A. Debus, C. De Oliveira, J. P. Duval, Y. Dietrich, M. El Ajjouri, C. Eisenmann, J. Gautier, R. Gebhardt, S. Grams, U. Helbig, C. Herbeaux, N. Hubert, C. Kitegi, O. Kononenko, M. Kuntzsch, M. LaBerge, S. Le, B. Leluan, A. Loulergue, V. Malka, F. Marteau, M. H. N. Guyen, D. Oumbarek-Espinos, R. Pausch, D. Pereira, T. Puschel, J. P. Ricaud, P. Rommeluere, E. Roussel, P. Rousseau, S. Schobel, M. Sebdaoui, K. Steiniger, K. Tavakoli, C. Thaury, P. Ufer, M. Valleau, M. Vandenberghe, J. Veteran, U. Schramm, and M. E. Couprie, "Seeded free-electron laser driven by a compact laser plasma accelerator," Nat. Photonics **17**, 150–156 (2023).
[49]O. Lundh, J. Lim, C. Rechatin, L. Ammoura, A. Ben-Ismail, X. Davoine, G. Gallot, J. P. Goddet, E. Lefebvre, V. Malka, and J. Faure, "Few femtosecond, few kiloampere electron bunch produced by a laser-plasma accelerator," Nat. Phys. **7**, 219–222 (2011).
[50]O. Zarini, J. C. Cabadağ, Y. Y. Chang, A. Kohler, T. Kurz, S. Schobel, W. Seidel, M. Bussmann, U. Schramm, A. Irman, and A. Debus, "Multioctave high-dynamic range optical spectrometer for single-pulse, longitudinal characterization of ultrashort electron bunches," Phys. Rev. Accel. Beams **25**, 012801 (2022).
[51]Q. K. Jia, "Analysis of emissions from prebunched electron beams," Phys. Rev. Accel. Beams **20**, 070702 (2017).
[52]C. Emma, X. Xu, A. Fisher, R. Robles, J. P. MacArthur, J. Cryan, M. J. Hogan, P. Musumeci, G. White, and A. Marinelli, "Terawatt attosecond X-ray source driven by a plasma accelerator," APL Photonics **6**, 10 (2021).
[53]D. Xiang and W. Wan, "Generating ultrashort coherent soft X-ray radiation in storage rings using angular-modulated electron beams," Phys. Rev. Lett. **104**, 084803 (2010).
[54]C. Feng, D. Xiang, H. X. Deng, D. Z. Huang, D. Wang, and Z. T. Zhao, "Generating intense fully coherent soft x-ray radiation based on a laser-plasma accelerator," Opt. Express **23**, 14993–15002 (2015).
[55]K. Feng, C. H. Yu, J. S. Liu, W. T. Wang, Y. Tian, Z. J. Zhang, R. Qi, M. Fang, J. Q. Liu, Z. Y. Qin, Y. Wu, Y. Chen, L. T. Ke, C. Wang, and R. X. Li, "Coherent X-ray source generation with off-resonance laser modulation," Opt. Express **26**, 19067–19079 (2018).
[56]S. Shin, "New era of synchrotron radiation: Fourth-generation storage ring," AAPPS Bull. **31**, 21 (2021).
[57]S. V. Kutsaev, "Novel technologies for compact electron linear accelerators (review)," Instrum. Exp. Tech. **64**, 641–656 (2021).
[58]A. W. Chao, K. H. Mess, M. Tigner, and F. Zimmermann, Handbook of Accelerator Physics and Engineering (World Scientific, 2013).
[59]R. Lehe, M. Kirchen, I. A. Andriyash, B. B. Godfrey, and J.-L. Vay, "A spectral, quasi-cylindrical and dispersion-free particle-in-cell algorithm," Comput. Phys. Commun. **203**, 66–82 (2016).
[60]S. Jalas, I. Dornmair, R. Lehe, H. Vincenti, J. L. Vay, M. Kirchen, and A. R. Maier, "Accurate modeling of plasma acceleration with arbitrary order pseudo-spectral particle-in-cell methods," Phys. Plasmas **24**, 033115 (2017).
[61]C. Widmann, V. A. Rodriguez, N. Braun, M. Nicolai, and A. S. Mueller, "Beam transport system from a laser wakefield accelerator to a transverse gradient undulator," in *Proceedings of the 5th International Particle Accelerator Conference, IPAC2014, Dresden, Germany, 2014*, (JACoW, Geneva), 2014, p. THOBA03.
[62]T. Liu, T. Zhang, D. Wang, and Z. R. Huang, "Compact beam transport system for free-electron lasers driven by a laser plasma accelerator," Phys. Rev. Accel. Beams **20**, 020701 (2017).
[63]I. Agapov, G. Geloni, S. Tomin, and I. Zagorodnov, "OCELOT: A software framework for synchrotron light source and FEL studies," Nucl. Instrum. Methods Phys. Res., Sect. A **768**, 151–156 (2014).
[64]K. Floettmann, "A space charge tracking algorithm astra," https://www.desy.de/~mpyflo/, DESY, 2007.
[65]A. A. Zholents and M. S. Zolotorev, "Attosecond x-ray pulses produced by ultra short transverse slicing via laser electron beam interaction," New J. Phys. **10**, 025005 (2008).
[66]A. Fallahi, A. Yahaghi, and F. X. Kartner, "MITHRA 1.0: A full-wave simulation tool for free electron lasers," Comput. Phys. Commun. **228**, 192–208 (2018).
[67]Z. R. Huang, Y. T. Ding, and C. B. Schroeder, "Compact X-ray free-electron laser from a laser-plasma accelerator using a transverse-gradient undulator," Phys. Rev. Lett. **109**, 204801 (2012).
[68]K. Feng, C. H. Yu, J. S. Liu, W. T. Wang, Z. J. Zhang, R. Qi, M. Fang, J. Q. Liu, Z. Y. Qin, Y. Wu, Y. Chen, L. T. Ke, C. Wang, and R. X. Li, "Dispersion effects on performance of free-electron laser based on laser wakefield accelerator," High Power Laser Sci. Eng. **6**, e64 (2018).